ADVANCED OPTICAL MATERIALS
www.advopticalmat.de

Check for updates

21951071, 0, Downloaded from https://onlinelibrary.wiley.com/doi/10.1002/adom.202202824 by Westlake University, Wiley Online Library on [26/02/2023]. See the Terms and Conditions (https://onlinelibrary.wiley.com/terms-and-conditions) on Wiley Online Library for rules of use; OA articles are governed by the applicable Creative Commons License

A Universal Approach to High-Index-Contrast Flexible Integrated Photonics

*Zequn Chen, Yilin Shi, Maoliang Wei, Ye Luo, Hui Ma, Renjie Tang, Yang Weng, Hao Dai, Chuyu Zhong, Chunlei Sun, Lichun Wang, Ke Si, Wei Gong, Hongtao Lin, and Lan Li**

Flexible integrated photonics is an essential technology for emerging applications, including flexible optical interconnects, optogenetic stimulation, and implantable conformal sensing. Here, a novel and universal route for fabricating flexible photonic components with high-refractive-index contrast is reported. Central to such a unique method is the utilization of germanium oxide (GeO) as the sacrificial layer for releasing nanostructures from rigid substrates to flexible substrates. Various high-quality inorganic optical materials can be grown directly on GeO by different thin-film deposition methods due to its resistance to both high temperature and high-power oxygen plasmas. In addition to the absence of restrictions on the material choices and integration processes for flexible photonic structures, the approach uses water as the etchant to remove the sacrificial layer, which has minimal impact on the optical performance of the photonic structures. Using this approach, a strain-insensitive/sensitive microring resonator based on plasma-enhanced chemical vapor deposited silicon nitride and reactive sputtered titanium oxide, respectively, is demonstrated, establishing the strategy as a facile and universal route for the fabrication of high-index-contrast flexible integrated photonic devices with various functionalities.

1. Introduction

Unlike rigid optical devices, flexible photonic devices can be bent, folded, stretched, and twisted. By operating in various states, devices can be regulated and controlled to optimize their unique optical properties. Therefore, flexibility in photonics offers great advantages and potential applications in a wide range of unconventional and emerging fields, including photonic skin,[1] conformal sensing,[2,3] optogenetic stimulation probes,[4–7] optical communication,[8–12] etc.

Polymers have been commonly used to fabricate flexible photonic devices due to their natural flexibility and low-temperature film deposition.[13–15] However, a low-refractive-index contrast between the polymer core structures and cladding substrates cannot allow strong optical confinement, which often leads to the large size of the fabricated devices and is not conducive to high-density integration. In comparison with polymers, silicon-based materials,[16] inorganic oxides,[17,18] and chalcogenide glass[19] materials show high refractive index and low absorption loss, enabling a large degree of freedom in obtaining functional optical structures for strong optical confinement on flexible substrates.[20–23] It is innately advantageous to realize compact, flexible photonic devices using an inorganic-organic hybrid structure consisting of inorganic core material and organic cladding substrate.[24]

Nowadays, the manufacturing processes of high-index-contrast (HIC) flexible integrated photonic devices are based on pattern transfer[25–27] and monolithic integration.[16,28] Among the many materials used for flexible photonics, silicon-based flexible devices were prepared by transferring nanostructures from a rigid carrier wafer to the flexible substrate via under-cut etching of the sacrificial oxide layer.[26,27] Hydrofluoric acid (HF) is often used during this process, which etches optical films like silicon nitride (SiN), resulting in device degradation.[26]

Z. Chen
College of Optical Science and Engineering
Zhejiang University
Hangzhou, 310027, China

Z. Chen, Y. Shi, Y. Luo, R. Tang, Y. Weng, C. Sun, L. Li
Key Laboratory of 3D Micro/Nano Fabrication and Characterization of Zhejiang Province
School of Engineering
Westlake University
Hangzhou 310030, China
E-mail: lilan@westlake.edu.cn

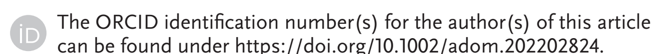
The ORCID identification number(s) for the author(s) of this article can be found under https://doi.org/10.1002/adom.202202824.

DOI: 10.1002/adom.202202824

Z. Chen, Y. Shi, Y. Luo, R. Tang, Y. Weng, C. Sun, L. Li
Institute of Advanced Technology
Westlake Institute for Advanced Study
Hangzhou 310024, China

M. Wei, H. Ma, H. Dai, C. Zhong, L. Wang, H. Lin
State Key Laboratory of Modern Optical Instrumentation
College of Information Science and Electronic Engineering
Zhejiang University
Hangzhou 310027, China

K. Si, W. Gong, H. Lin
MOE Frontier Science Center for Brain Science & Brain-Machine Integration
Zhejiang University
Hangzhou 310027, China

© 2023 Wiley-VCH GmbH

Directly depositing thin films on flexible substrates is another way to prepare flexible integrated photonic devices. However, SiN thin films[29,30] are usually deposited by plasma-enhanced chemical vapor deposition (PECVD) and low-pressure chemical vapor deposition (LPCVD).[31] LPCVD SiN thin film is usually deposited at high temperatures (≥800 °C), and PECVD SiN thin film deposition is typically performed at relatively low temperatures, like 350 °C. Although low temperatures are beneficial for reducing stress in films, they do not promote high density and smooth roughness, nor are they conducive to preparing films with low optical loss around telecommunication wavelengths due to residual functional groups such as Si—H and N—H bonds. Therefore, to obtain high-quality SiN thin films and reduce the propagation loss, subsequent annealing (400–1200 °C) is required for dehydrogenation and densification.[31,32] Flexible polymer substrates, however, generally cannot withstand such high temperatures (**Figure 1**a). While amorphous silicon (a-Si) devices[16] can be prepared by low-temperature deposition technology, there will be a large number of defects and Si—H bonds in the obtained thin films, resulting in a high optical loss around telecommunication wavelengths.[16,31] Magnetron sputtering inorganic oxides and functional glasses deposited at room temperature could provide a feasible route for the monolithic integration of devices on flexible substrates. However, the high-power oxygen plasma may somewhat damage polymer substrates (Figure 1b).[18] In addition, thermal evaporation can also be considered a near-room temperature film deposition technique to fabricate flexible integrated photonic devices directly.[12,28,33] However, this technique is only limited to materials with low melting points, such as chalcogenide glasses, which cannot be used in biophotonic applications due to the high toxicities of chalcogens.[34]

To address these issues, we develop a novel fabrication route for flexible integrated photonic devices using water-soluble germanium oxide (GeO) as the sacrificial layer, which can withstand high annealing temperatures and high-power oxygen plasma, allowing direct integration of inorganic optical materials via different thin-film deposition techniques. As a demonstration of this approach's universality, PECVD SiN and reactive sputtered titanium dioxide (TiO_2) were prepared separately for flexible photonic integration. Taking these materials as examples, our approach can be easily applied to other inorganic films by different deposition methods with tailored optical characteristics to meet the requirements for various applications. Moreover, GeO can be dissolved in water, avoiding unnecessary acid corrosion while releasing optical structures from the rigid substrate to the flexible one. Combining this universal fabrication method with the multiple neutral-axis theory,[28] we designed and prepared a series of high-performance HIC flexible integrated photonic devices and demonstrated their potential applications as robust, sensitive strain sensors. In addition to flexible waveguide integrated devices, we believe this method

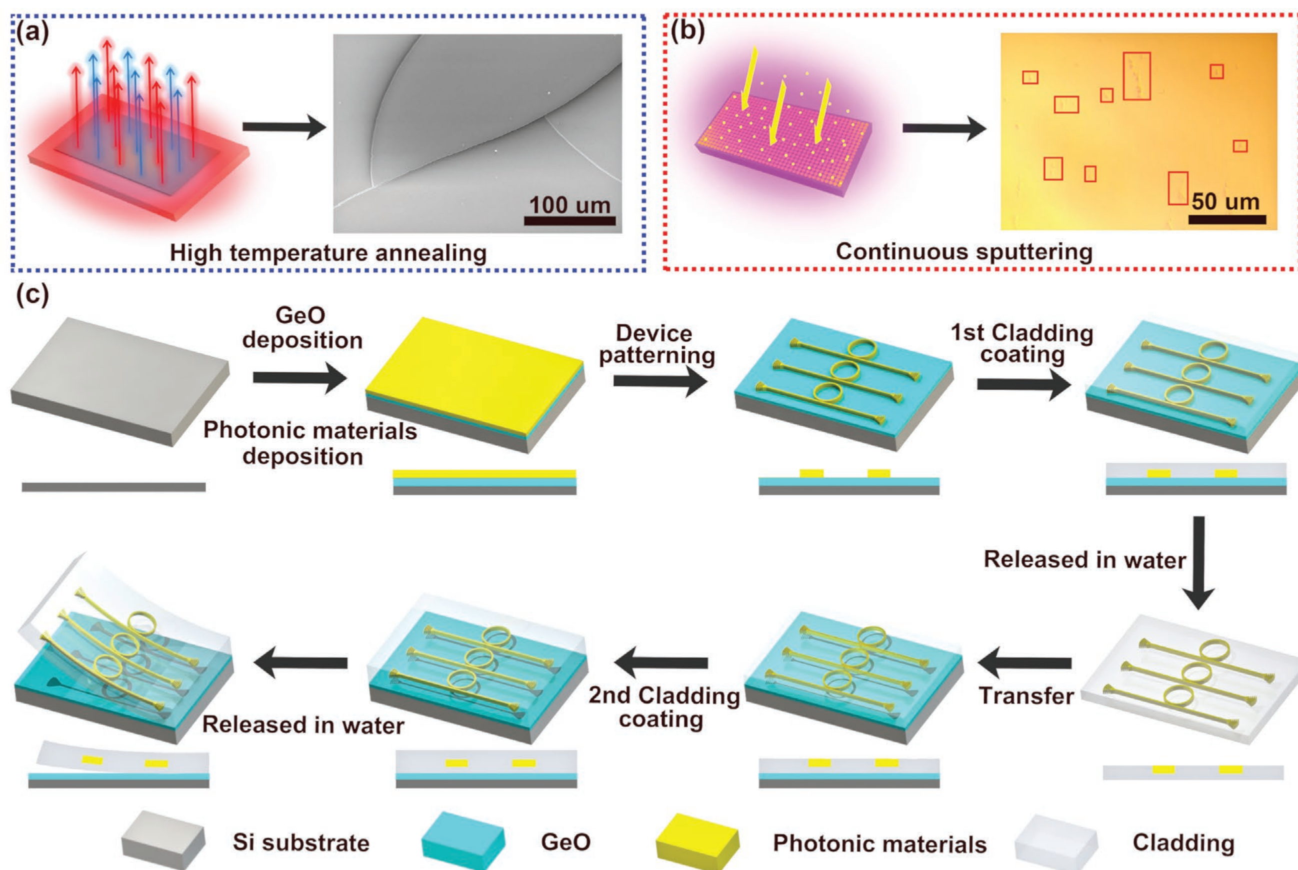

Figure 1. Damage to the flexible polymer substrate during thin film deposition after a) high-temperature annealing and by b) reactive sputtering, respectively. c) Schematic diagram of the device fabrication process.

© 2023 Wiley-VCH GmbH

21951071, 0, Downloaded from https://onlinelibrary.wiley.com/doi/10.1002/adom.202202824 by Westlake University, Wiley Online Library on [26/02/2023]. See the Terms and Conditions (https://onlinelibrary.wiley.com/terms-and-conditions) on Wiley Online Library for rules of use; OA articles are governed by the applicable Creative Commons License

can also be applied to the fabrication of other flexible inorganic nanophotonic structures, such as dielectric metasurfaces,[35,36] high contrast gratings,[37] epsilon-near-zero media,[38,39] hyperbolic metamaterials structures,[40] etc. Due to the discrete configuration of these structures in polymer substrates, the dielectric material is more easily relieved in the etchant for flexible devices. This novel technology breaks the limitation of material selection in the fabrication process of flexible integrated photonic devices, dramatically simplifies and improves fabrication efficiency and yield, and provides possibilities for the applications mentioned above.

2. Results and Discussion

2.1. Optimization of the Thin Film Deposition for Sacrificial and Optical Layers

Figure 1c illustrates our fabrication process for flexible integrated photonic devices. Experimental details are provided in the Supporting Information. First, we optimized the reactive sputtering deposition condition of GeO thin films to meet the need for a high-quality sacrificial layer and the following optical thin films. The oxygen flow rate plays an important role in the quality control of the deposited film. As shown in **Figure 2**a, the deposition rate drops dramatically when the oxygen flow rate goes up to 5.5 sccm, which we refer to as the "knee point." In the case of a small amount of oxygen flow, the deposition rate is rapid, but the thin film produced by reactive sputtering is anoxic. Excessive oxygen flow would lead to poisoning on the surface of the target and reduce the deposition rate; thus, we chose to conduct the GeO sputtering at an oxygen flow of 6 sccm, slightly over the "knee point." Figure 2b,c shows that the surface roughness of obtained GeO thin films increases with increasing working pressure and radio frequency (RF) power, respectively. However, low deposition power means a low deposition rate. Therefore, to obtain a small roughness at a certain rate, the optimal GeO thin film has been prepared at the reactor pressure of 0.3 pa, RF power of 100 W, and the mixed gases of Ar/O_2 (35/6 sccm) (deposition rate: ≈0.8 Å s^{-1}) followed by thermal annealing at 550 °C for 6 h in the muffle furnace. The root-mean-square (RMS) roughness of the GeO thin film surface determined by Atomic Force Microscopy (AFM) is 0.42 ± 0.02 nm, as shown in Figure 2d. The optimal film thickness for the sacrificial layer depends on the rate at which GeO dissolves in water. It could take longer to release optical structures from a rigid substrate to a flexible substrate if the GeO thickness is too thin. For example, using 200 nm thick GeO as the sacrificial layer requires 2–3 days, whereas using 600 nm thick GeO only requires less than one day to completely release the nanostructures. Further increasing GeO thickness will have a limited impact on reducing the time for device fabrication since it will prolong the sputtering deposition time of GeO. Moreover, as GeO thickness increases, the roughness of the surface will increase, adversely affecting other materials deposited on GeO. Therefore, the thickness of the sacrificial layer is chosen to be 650 nm with relatively small roughness and short structure release time.

To demonstrate the universality of integration techniques on GeO thin films, SiN and TiO_2 were deposited on GeO thin films by PECVD and reactive sputtering, respectively, to ensure that this approach is compatible with high deposition

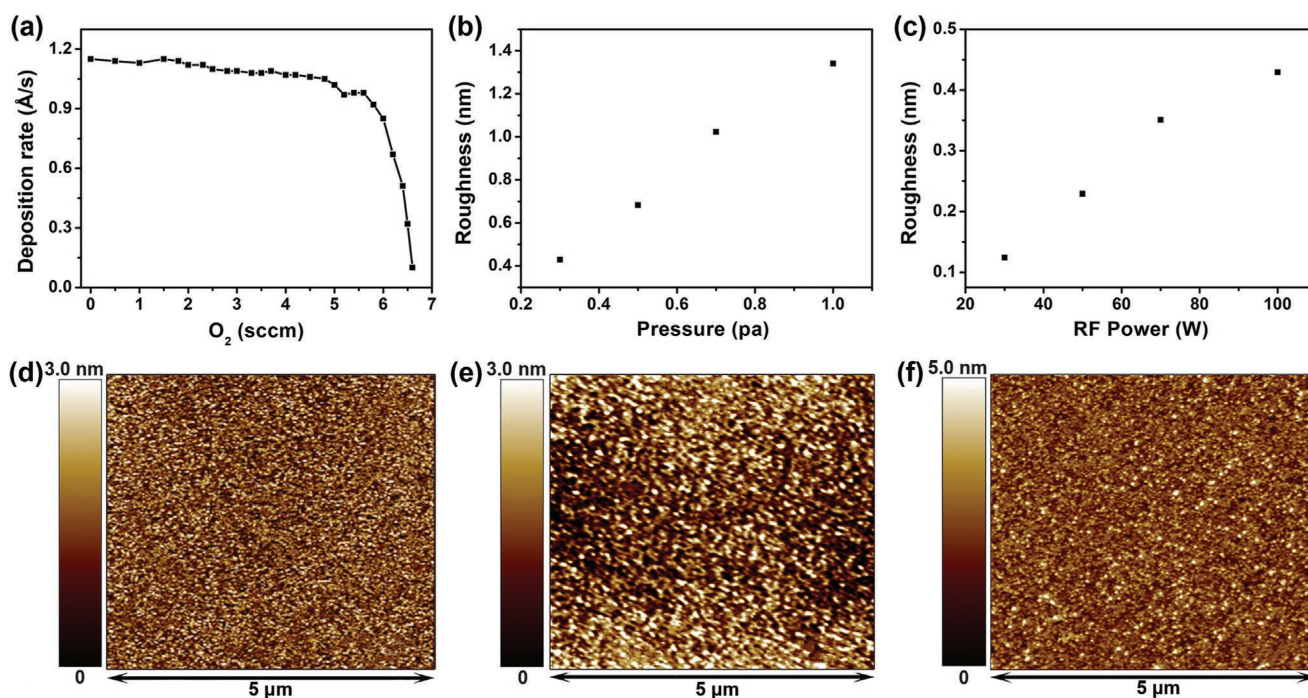

Figure 2. Optimization of sputtering parameters for GeO thin films. a) Deposition rates of GeO as a function of oxygen flow rates. Surface roughness of GeO thin film deposited at different b) working pressure, and c) RF power, respectively. AFM images of d) GeO thin film (RMS = 0.42 ± 0.02 nm), e) SiN thin films (RMS = 0.86 ± 0.15 nm), and f) TiO_2 thin films (RMS = 1.20 ± 0.03 nm) on GeO thin films.

© 2023 Wiley-VCH GmbH

21951071, 0, Downloaded from https://onlinelibrary.wiley.com/doi/10.1002/adom.202202824 by Westlake University, Wiley Online Library on [26/02/2023]. See the Terms and Conditions (https://onlinelibrary.wiley.com/terms-and-conditions) on Wiley Online Library for rules of use; OA articles are governed by the applicable Creative Commons License

temperatures and high oxygen plasmas. The surface roughness of SiN and TiO_2 thin films deposited on the GeO is 0.86 ± 0.15 nm and 1.20 ± 0.03 nm, respectively (Figure 2e,f). The refractive indices and absorption coefficients are also characterized by ellipsometry, as shown in Figure S1 (Supporting Information), indicating low optical loss over a broad wavelength range. Thus our optimized GeO thin film is compatible with most deposition processes and could be regarded as a robust sacrificial substrate layer to prepare inorganic optical films, which facilitates the fabrication of low-loss HIC flexible photonic devices with the added water-soluble nature of GeO thin films.

2.2. Flexible Integrated Photonic Devices Based on PECVD SiN

CMOS-compatible SiN has received increasing attention for sensing, communication, imaging, computation, and bioapplications due to its superior optical properties, including broadband transparency, large nonlinearity, and biocompatibility. Low-loss SiN thin films are usually prepared under high-power plasma conditions and may require annealing around 1200 °C for dehydrogenation and densification.[32] However, polymers that are usually used as flexible substrates cannot withstand high temperatures. Even though some polyimide films can be used at temperatures as high as 400 °C,[41] direct deposition of PECVD SiN may introduce additional damage to the polymer substrate and unwanted carbon contamination in the chamber.[41] To construct HIC flexible SiN photonic devices, sacrificial layers are adopted to transfer nanostructures patterned on the rigid carrier to the flexible substrate. SiO_2 has been used and etched by HF to fabricate flexible SiN microring resonators (MRRs), in which the acid etchant etches SiN and polymer materials, such as PDMS[42] as shown in Figure S2 (Supporting Information).

Here, we demonstrate a new flexible SiN waveguide integration platform comprising SiN at the center of symmetrically coated PDMS, as shown in **Figure 3**a. The preparation details are described in Section S1 and Figure S3 (Supporting Information). A sacrificial layer of GeO and a DI water etchant were used in the preparation process without causing corrosion to the device. The width and height of the SiN waveguide is 1 and 500 nm, respectively, which supports the fundamental TE mode (Figure 3b). The whole device consists of grating couplers and MRRs, as shown in Figure 3c,d. The magnified views of the surface morphologies in Figure 3e,f show the smoothness of the waveguide sidewall, indicating an optimized process for lithography patterning (Figure S4, Supporting Information) and ICP-RIE etching. The measurement platform and system are shown in Figure 3g and Figure S5 (Supporting Information). To test the flexible SiN MRRs, the grating couplers and fibers were efficiently coupled with 8° tilt, and the transmission spectrum was collected by a broadband tunable laser system (Santec full-band TSL-550). The MRRs are located at the bottom of the bend center. Different bending radii of flexible photonic devices could be realized by moving the stage left and right. SiN is located on the neutral axis of the whole device because the PDMS thickness of the top and bottom cladding layers is as consistent as possible. In the neutral axis position, the strain upon bending vanishes. Figure 3h shows

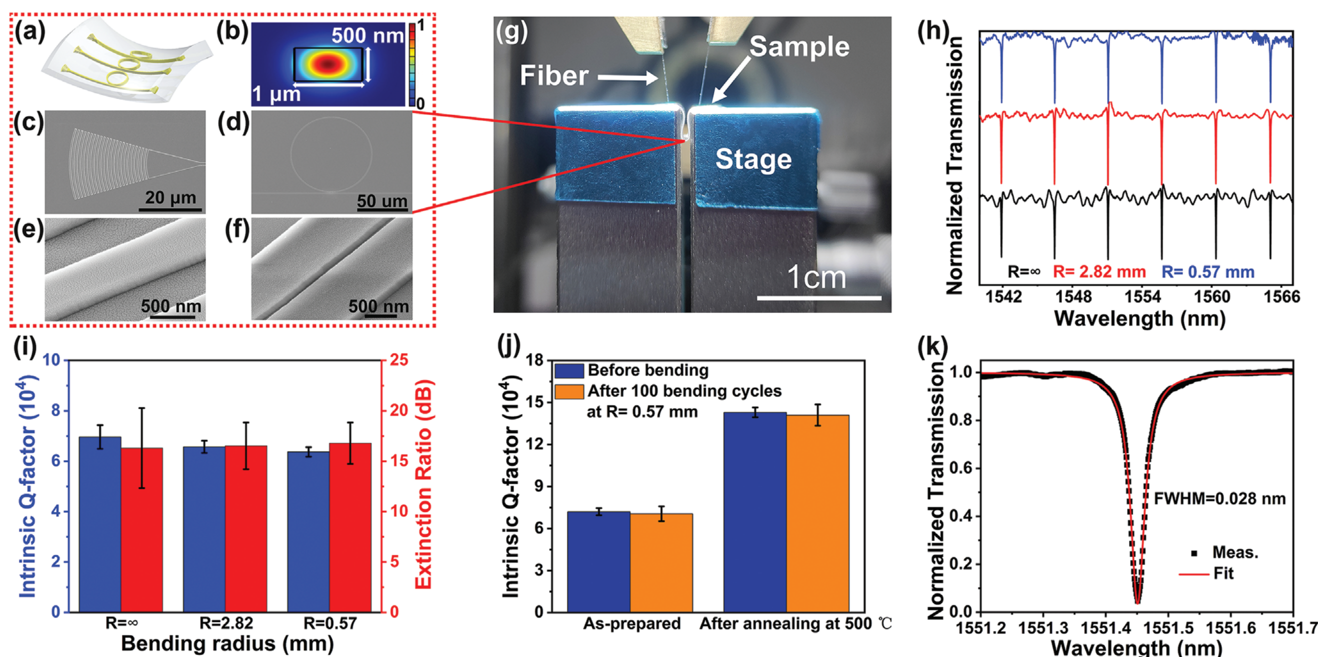

Figure 3. Flexible integrated photonic devices based on PECVD SiN. a) Schematic diagram of the fabricated device. b) Simulated fundamental TE-polarized mode profile at 1550 nm. SEM images of the c) grating coupler and d) MRR. e,f) Magnified views show the details of the surface morphology of the grating coupler and MRR, respectively. g) Photo of the device under measurement at a bending radius of 0.57 mm. h) Normalized optical transmission spectra of flexible SiN MRR at different bending radii. i) Intrinsic *Q* factors and extinction ratios of the flexible SiN MRRs at different bending radii. j) Thermal and mechanical stability tests. k) Normalized optical transmission spectra of the flexible SiN MRR after 100 bending cycles at $R = 0.57$ mm.

© 2023 Wiley-VCH GmbH

21951071, 0, Downloaded from https://onlinelibrary.wiley.com/doi/10.1002/adom.202202824 by Westlake University, Wiley Online Library on [26/02/2023]. See the Terms and Conditions (https://onlinelibrary.wiley.com/terms-and-conditions) on Wiley Online Library for rules of use; OA articles are governed by the applicable Creative Commons License

the transmission spectra of the flexible SiN MRRs under different bending radii following the neutral axis design.[28] As a result, the resonant dip of SiN MRRs barely moves at different bending radii. The intrinsic quality factors (Q_{int}) and extinction ratios of the device remain minimal variations under different bending radii, indicating robust mechanical reliability (Figure 3i).

The SiN thin film prepared by PECVD at 350 °C is not dense, and there may be some defects and dangling bonds of Si—H and N—H, which causes the intrinsic optical loss of the film.[32,43,44] The Q_{int} value of the 350 °C SiN MRR is only 7.0×10^4, corresponding to a propagation loss of 5.3 dB cm^{-1}. After being annealed at 500 °C, the Q_{int} value of the flexible SiN MRR is up to 1.4×10^5, corresponding to a propagation loss of 2.6 dB cm^{-1} (Figure 3j,k), comparable to some rigid SiN MRR devices listed in Table S1 (Supporting Information). After 100 times bending cycles, the Q_{int} of the SiN MRR shows few changes, indicating superior mechanical robustness of the flexible SiN MRR device (Figure 3j). Therefore, our method has proved that it could not only realize the fabrication of flexible HIC photonics from materials requiring high-temperature deposition but also maintain superior device performance while greatly simplifying the process steps and improving the yield. And such a symmetrical structure design, in which the optical characteristics remain well under mechanical deformation, holds great potential for conformal optical sensing[19,27,45] and bioapplications such as flexible brain machine photonic probes,[4,46] optical cochlea,[47,48] etc.

2.3. Flexible Integrated Photonic Devices Based on Reactive Sputtered TiO_2

As described above, the flexible polymer substrate might be damaged under continuous high-power oxygen plasma conditions (Figure 1b). To further verify that high-quality reactive sputtered oxide or glasses can also be applied for HIC flexible photonic devices, we chose TiO_2 to demonstrate the universality of our fabrication method. That is because that TiO_2 also holds excellent properties, including low optical loss, wide transparency window, high refractive index, and large negative thermo-optic coefficient, which allows efficient and compact modulation and switching in flexible photonic circuits.[17] Instead of using a symmetry structure to construct flexible MRRs without being influenced by external mechanical deformation, MRRs can be used as sensitive bendable and stretchable strain sensors by placing the device in a multilayer structure, in which multiple neutral planes can be generated for different functions use. Our previous work[28,49] quantitatively analyzed the strain-optical coupling mechanism.

Hence, we deposited TiO_2 thin films on GeO thin films by reactive sputtering under 400 W, and designed and fabricated flexible TiO_2 MRRs strain sensors with a multi-neutral axis structure. The preparation details are in Section S1 (Supporting Information). The flexible device diagram is shown in **Figure 4**a. The flexible photonic chip (from bottom to top) consists of a polyimide substrate, a silicone adhesive, and a SU-8 cladding layer in which the TiO_2 MRRs are embedded.

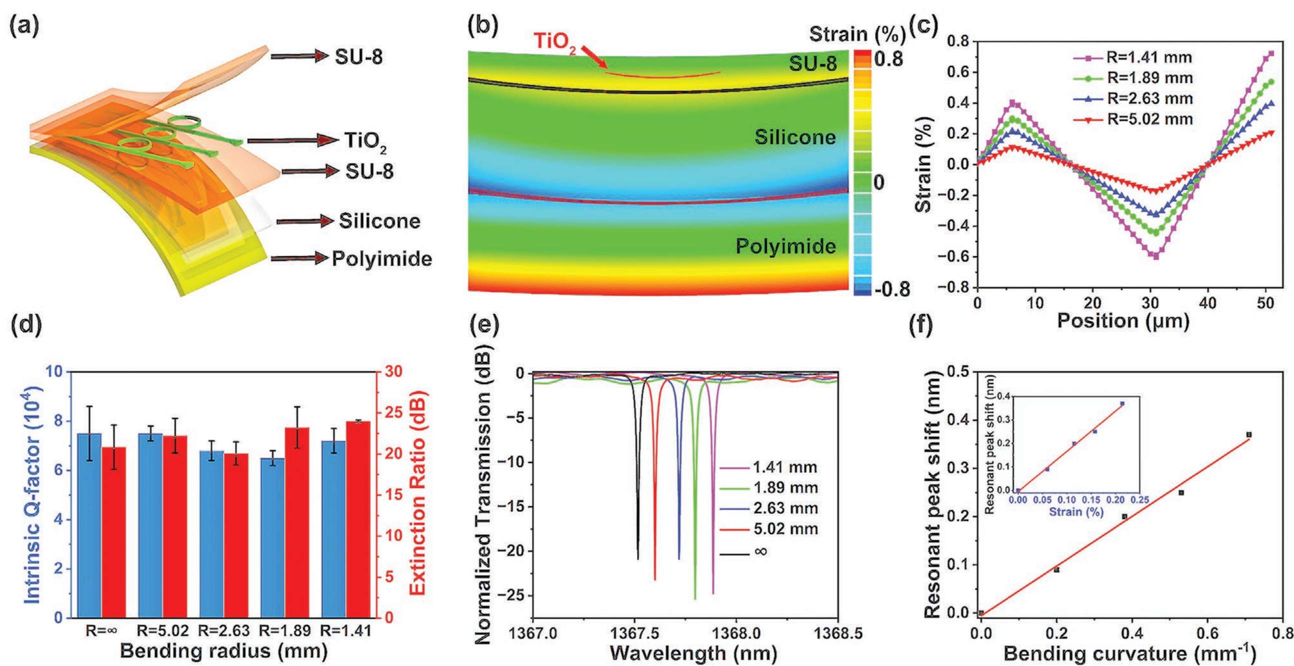

Figure 4. Flexible integrated photonic devices based on reactive sputtered TiO_2. a) Schematic diagram of the fabricated device. b) Strain distribution in the multilayer laminated photonic chip structure during bending at $R = 1.4$ mm. The red line represents the position of the TiO_2 MRR. c) Strain along the structure's center with a SU-8 layer thickness of 6 μm calculated using FEM illustrating the analytical multi-neutral-axis model at different bending radii. d) Intrinsic Q factors and extinction ratios of the flexible TiO_2 MRR at different bending radii. e) Normalized optical transmission spectra of the flexible TiO_2 MRR at different bending radii. f) Resonance wavelength peak shift plotted as a function of the bending curvature. The inset: resonance wavelength peak shift plotted as a function of bending strain, which can be calculated from the bending curvature.

© 2023 Wiley-VCH GmbH

21951071, 0, Downloaded from https://onlinelibrary.wiley.com/doi/10.1002/adom.202202824 by Westlake University, Wiley Online Library on [26/02/2023]. See the Terms and Conditions (https://onlinelibrary.wiley.com/terms-and-conditions) on Wiley Online Library for rules of use; OA articles are governed by the applicable Creative Commons License

21951071, 0, Downloaded from https://onlinelibrary.wiley.com/doi/10.1002/adom.202202824 by Westlake University, Wiley Online Library on [26/02/2023]. See the Terms and Conditions (https://onlinelibrary.wiley.com/terms-and-conditions) on Wiley Online Library for rules of use; OA articles are governed by the applicable Creative Commons License

The insertion of silicone with a low modulus between the two relatively rigid plastics (SU-8 and polyimide) is an excellent strain-releasing agent in our local multiple-neutral axis design. Due to the soft silicone interlayer, the neutral axis position can be shifted from the center to the near-surface of the stack within the SU-8 layer. Thus, the neutral axis can be controlled by changing the thickness of the top and bottom SU-8 coating, which allows evanescent interactions between the optical field and the surrounding environment while showing remarkable-mechanical flexibility.[28] Figure 4b plots the strain distribution of the prepared device simulated by the finite element method (FEM)[28,33] with a bending radius of 1.4 mm. The simulation results show that the peak strain at the position of TiO_2 MRR is 0.21%. And the strain increases gradually with the decrease of the bending radius (Figure 4c). The Q_{int} value and extinction ratio of the device exhibits a small range of variations under different bending radii, illustrating the mechanical reliability. And the Q_{int} value ranges from $6.3–7.5 \times 10^4$ under different bending radii (Figure 4d), indicating optical performance improvement compared with previously reported work on flexible TiO_2 MRRs.[18] Because the TiO_2 MRR is not located at the neutral axis, the local strain at the TiO_2 MRR changes as the chip is bent. Figure 4e clearly shows the redshift of TiO_2 MRR dip wavelength with the decrease of bending radius. The TiO_2 MRR peak wavelength shift plotted as a function of bending curvature is presented in Figure 4f. When the bending curvature of the horizontal axis in Figure 4f is converted into bending strain,[28] the relationship between TiO_2 MRR peak wavelength drift and strain is shown in the inset of Figure 4f, which proves the linear dependence of formant displacement on the mechanical strain.[28] Therefore, our approach can also achieve the preparation of flexible photonic devices with multi-neutral axis structures comparable to the previous reports.[28] However, the difference is that our method can accommodate most materials and is not limited by the thin film deposition process. The significant variation of the strain-induced formant wavelength shift provides a strategy for strain-optical coupling in flexible integrated photonic devices, which has great potential applications in the field of photonic tuning and strain sensing.[50]

3. Conclusions

In conclusion, we have experimentally demonstrated a simple and universal method for fabricating flexible HIC integrated photonic devices. Different from the traditional approaches, which rely on HF etching of silicon oxide and multi-step pattern transfer, this method takes advantage of the characteristics that GeO is soluble in water and can withstand high temperature and high-power oxygen plasma. As a result, it is a non-destructive process of device preparation and significantly improves device performance, processing throughput, and yield. In addition to simplifying the device integration fabrication process, guided by multi-neutral axis theory, we demonstrate flexible devices with extremely high flexibility and mechanical robustness, despite the inherent mechanical fragility of these inorganic material thin films. The fabricated devices can sustain a submillimeter bending radius without affecting their optical properties. As an example, we have implemented the fabrication of a flexible SiN waveguide-integrated MRR device with a Q_{int}-value comparable to that of rigid photonic devices. Furthermore, by changing the thickness of the up and bottom SU-8 cladding layers, the TiO_2 MRR device is placed slightly away from the neutral axis position, and the strain-optical coupling behavior is analyzed. We anticipate that this unique and universal fabrication strategy will significantly accelerate and expand the development and applications of flexible HIC photonic devices for novel photonic functions.

4. Experimental Section

Experimental details are listed in the Supporting Information.

Supporting Information

Supporting Information is available from the Wiley Online Library or from the author.

Acknowledgements

This work was financially supported by the National Natural Science Foundation of China (62175202 and 12104375); Zhejiang Provincial Natural Science Foundation of China (LD22F040002); Leading Innovative and Entrepreneur Team Introduction Program of Zhejiang (2020R01005); and MOE Frontier Science Center for Brain Science & Brain-Machine Integration, Zhejiang University. The authors would like to acknowledge Westlake Center for Micro/Nano Fabrication and Instrumentation, Service Center for Physical Sciences (Lin Liu's help in AFM characterization, Zhen Yang's assistance in SEM characterization, and Ying Nie's help in thermal annealing) at Westlake University, and ZJU Micro-Nano Fabrication Center at Zhejiang University for the facility support. The authors would also like to thank Xue Wang, Qing Zhao, and Liming Shan for their help in device fabrication.

Conflict of Interest

The authors declare no conflict of interest.

Data Availability Statement

The data that support the findings of this study are available from the corresponding author upon reasonable request.

Keywords

flexible photonics, universal fabrication approach, high-index contrast photonics, ring resonators

Received: November 26, 2022
Revised: January 24, 2023
Published online:

[1] C. Zhang, H. Dong, C. Zhang, Y. Fan, J. Yao, Y. S. Zhao, *Sci. Adv.* **2021**, *7*, 3530.
[2] L. Gao, Y. Zhang, V. Malyarchuk, L. Jia, K.-I. Jang, R. Chad Webb, H. Fu, Y. Shi, G. Zhou, L. Shi, D. Shah, X. Huang, B. Xu, C. Yu, Y. Huang, J. A. Rogers, *Nat. Commun.* **2014**, *5*, 4938.

 © 2023 Wiley-VCH GmbH

[3] W. Peng, Q. Liao, H. Song, *Nanoscale Res. Lett.* **2021**, *16*, 23.
[4] Z. Chen, L. Li, *Acc. Mater. Res.* **2021**, *2*, 315.
[5] S. Park, Y. Guo, X. Jia, H. K. Choe, B. Grena, J. Kang, J. Park, C. Lu, A. Canales, R. Chen, Y. S. Yim, G. B. Choi, Y. Fink, P. Anikeeva, *Nat. Neurosci.* **2017**, *20*, 612.
[6] M. H. Du, L. Huang, J. J. Zheng, Y. Xi, Y. Dai, W. D. Zhang, W. Yan, G. M. Tao, J. R. Qiu, K. F. So, C. R. Ren, S. F. Zhou, *Adv. Sci.* **2020**, *7*, 2001410.
[7] Z. Zhao, E. Kim, H. Luo, J. Zhang, Y. Xu, *J. Micromech. Microeng.* **2017**, *28*, 015012.
[8] T. Wang, D. Zheng, J. Zhang, J. Qiao, C. Min, X. Yuan, M. Somekh, F. Feng, *Adv. Funct. Mater.* **2022**, *32*, 2208694.
[9] D. Li, S. Yip, F. Li, H. Zhang, Y. Meng, X. Bu, X. Kang, C. Lan, C. Liu, J. C. Ho, *Adv. Opt. Mater.* **2020**, *8*, 2001201.
[10] X. Jin, Y. Sun, Q. Wu, Z. Jia, S. Huang, J. Yao, H. Huang, J. Xu, *ACS Appl. Mater. Interfaces* **2019**, *11*, 42385.
[11] N. Strobel, N. Droseros, W. Kontges, M. Seiberlich, M. Pietsch, S. Schlisske, F. Lindheimer, R. R. Schroder, U. Lemmer, M. Pfannmoller, N. Banerji, G. Hernandez-Sosa, *Adv. Mater.* **2020**, *32*, 1908258.
[12] L. Li, H. Lin, Y. Huang, R.-J. Shiue, A. Yadav, J. Li, J. Michon, D. Englund, K. Richardson, T. Gu, J. Hu, *Optica* **2018**, *5*, 44.
[13] M. Choi, J. W. Choi, S. Kim, S. Nizamoglu, S. K. Hahn, S. H. Yun, *Nat. Photonics* **2013**, *7*, 987.
[14] S. T. Parker, P. Domachuk, J. Amsden, J. Bressner, J. A. Lewis, D. L. Kaplan, F. G. Omenetto, *Adv. Mater.* **2009**, *21*, 2411.
[15] S. Chen, M. Zhuo, X. Wang, G. Wei, L. Liao, *PhotoniX* **2021**, *2*, 2.
[16] L. Fan, L. T. Varghese, Y. Xuan, J. Wang, B. Niu, M. Qi, *Opt. Express* **2012**, *20*, 20564.
[17] Z. Chen, M. Wei, Y. Luo, J. Jian, Y. Ye, Y. Yin, C. Sun, C. Zhong, K. Si, D. Zhang, H. Lin, L. Li, *Opt. Mater. Express* **2022**, *12*, 4061.
[18] L. Li, P. Zhang, W.-M. Wang, H. Lin, A. B. Zerdoum, S. J. Geiger, Y. Liu, N. Xiao, Y. Zou, O. Ogbuu, Q. Du, X. Jia, J. Li, J. Hu, *Sci. Rep.* **2015**, *5*, 13832.
[19] J. Michon, S. Geiger, L. Li, C. Goncalves, H. Lin, K. Richardson, X. Jia, J. Hu, *Photonics Res.* **2020**, *8*, 194.
[20] Y.-B. Kim, J.-W. Cho, Y.-J. Lee, D. Bae, S.-K. Kim, *Light: Sci. Appl.* **2022**, *11*, 316.
[21] M. Chin, C. Lee, S. Lee, S. Darmawan, *Appl. Opt.* **2005**, *44*, 3077.
[22] J. T. Robinson, K. Preston, O. Painter, M. Lipson, *Opt. Express* **2008**, *16*, 16659.
[23] A. Melloni, R. Costa, G. Cusmai, F. Morichetti, *Int. J. Mater. Prod. Technol.* **2009**, *34*, 421.
[24] Y. Zou, D. Zhang, H. Lin, L. Li, L. Moreel, J. Zhou, Q. Du, O. Ogbuu, S. Danto, J. D. Musgraves, K. Richardson, K. D. Dobson, R. Birkmire, J. Hu, *Adv. Opt. Mater.* **2014**, *2*, 478.
[25] H. C. Ko, M. P. Stoykovich, J. Song, V. Malyarchuk, W. M. Choi, C.-J. Yu, J. B. Geddes Iii, J. Xiao, S. Wang, Y. Huang, J. A. Rogers, *Nature* **2008**, *454*, 748.
[26] Y. Chen, M. Li, *Opt. Lett.* **2014**, *39*, 3449.
[27] Y. Chen, H. Li, M. Li, *Sci. Rep.* **2012**, *2*, 622.
[28] L. Li, H. Lin, S. Qiao, Y. Zou, S. Danto, K. Richardson, J. D. Musgraves, N. Lu, J. Hu, *Nat. Photonics* **2014**, *8*, 643.
[29] M. Dong, G. Clark, A. J. Leenheer, M. Zimmermann, D. Dominguez, A. J. Menssen, D. Heim, G. Gilbert, D. Englund, M. Eichenfield, *Nat. Photonics* **2021**, *16*, 59.
[30] G. Liang, H. Huang, A. Mohanty, M. C. Shin, X. Ji, M. J. Carter, S. Shrestha, M. Lipson, N. Yu, *Nat. Photonics* **2021**, *15*, 908.
[31] X. Ji, S. Roberts, M. Corato-Zanarella, M. Lipson, *APL Photonics* **2021**, *6*, 071101.
[32] X. Ji, F. A. S. Barbosa, S. P. Roberts, A. Dutt, J. Cardenas, Y. Okawachi, A. Bryant, A. L. Gaeta, M. Lipson, *Optica* **2017**, *4*, 619.
[33] Y. Luo, C. Sun, H. Ma, M. Wei, J. Li, J. Jian, C. Zhong, Z. Chen, R. Tang, K. A. Richardson, H. Lin, L. Li, *Opt. Express* **2022**, *30*, 26534.
[34] V. P. P. Schiar, D. B. dos Santos, D. S. Lüdtke, F. Vargas, M. W. Paixão, C. W. Nogueira, G. Zeni, J. B. T. Rocha, *Toxicol. In Vitro* **2007**, *21*, 139.
[35] S. M. Kamali, A. Arbabi, E. Arbabi, Y. Horie, A. Faraon, *Nat. Commun.* **2016**, *7*, 11618.
[36] Z. H. Jiang, L. Kang, D. H. Werner, *Nat. Commun.* **2017**, *8*, 356.
[37] J. Fernandes, Y. H. Kwon, J. J. Kim, H. Liu, H. Jiang, *J. Microelectromech. Syst.* **2018**, *27*, 599.
[38] Z. Hu, C. Chen, Z. Zhou, Y. Li, *IEEE Antennas Wirel. Propag. Lett.* **2020**, *19*, 1591.
[39] I. Liberal, A. M. Mahmoud, N. Engheta, *Nat. Commun.* **2016**, *7*, 10989.
[40] A. Poddubny, I. Iorsh, P. Belov, Y. Kivshar, *Nat. Photonics* **2013**, *7*, 948.
[41] H. Yuan, C. Lu, S. Zhang, G. Wu, *New Carbon Mater.* **2015**, *30*, 115.
[42] A. Mata, A. J. Fleischman, S. Roy, *Biomed. Microdevices* **2005**, *7*, 281.
[43] F. Ay, A. Aydinli, *Opt. Mater.* **2004**, *26*, 33.
[44] L. Wang, W. Xie, D. Van Thourhout, Y. Zhang, H. Yu, S. Wang, *Opt. Express* **2018**, *26*, 9645.
[45] O. M. Omisore, S. Han, J. Xiong, H. Li, Z. Li, L. Wang, *IEEE Trans. Syst. Man Cybern. Syst.* **2022**, *52*, 631.
[46] J. W. Reddy, M. Lassiter, M. Chamanzar, *Microsyst Nanoeng* **2020**, *6*, 85.
[47] A. Dieter, D. Keppeler, T. Moser, *EMBO Mol. Med.* **2020**, *12*, 11618.
[48] R. T. Richardson, A. C. Thompson, A. K. Wise, K. Needham, *Expert Opin. Biol. Ther.* **2017**, *17*, 213.
[49] L. Li, H. Lin, S. Qiao, Y.-Z. Huang, J.-Y. Li, J. Michon, T. Gu, C. Alosno-Ramos, L. Vivien, A. Yadav, K. Richardson, N. Lu, J. Hu, *Light: Sci. Appl.* **2018**, *7*, 17138.
[50] J. Guo, M. Niu, C. Yang, *Optica* **2017**, *4*, 1285.

 © 2023 Wiley-VCH GmbH

21951071, 0, Downloaded from https://onlinelibrary.wiley.com/doi/10.1002/adom.202202824 by Westlake University, Wiley Online Library on [26/02/2023]. See the Terms and Conditions (https://onlinelibrary.wiley.com/terms-and-conditions) on Wiley Online Library for rules of use; OA articles are governed by the applicable Creative Commons License